ACS OMEGA

Article

Cite This: ACS Omega 2020, 5, 274−280

http://pubs.acs.org/journal/acsodf

Studies on Magnetic and Dielectric Properties of Antiferromagnetically Coupled Dinuclear Cu(II) in a One-Dimensional Cu(II) Coordination Polymer

Srikanta Jana,[†,⊥] Apurba Ray,[‡,⊥] Angeera Chandra,[†] M. Salah El Fallah,[*,§] Sachindranath Das,[*,‡] and Chittaranjan Sinha[*,†]

[†]Department of Chemistry, and [‡]Department of Instrumentation Science, Jadavpur University, 700032 Kolkata, India

[§]Departament de Química Inorgànica i Organica, Secció de Química Inorgànica, Universitat de Barcelona, Martí i Franquès, 1-11, 08028 Barcelona, Spain

Supporting Information

ABSTRACT: A one-dimensional Cu(II) coordination polymer with encapsulated antiferromagnetically coupled binuclear Cu(II) has been synthesized by using 5-nitroisophthalic acid (5-N-IPA) and 4-aminopyridine (4-APY) $[Cu_2(5\text{-N-IPA})_2(4\text{-APY})_4]_n$ (**1**). Electrical properties are examined by complex impedance (Z^*), dielectric permittivity (ε^*), and ac conductivity studies at different frequencies (10 kHz−5 MHz) and temperatures (253−333 K). The contribution of grain and grain boundary has been explained by a different theoretical model. The variable temperature magnetic susceptibility data for compound **1** were recorded between 300 and 2 K. The shape of the curve ($\chi_M T$ vs T) indicates dominant antiferromagnetic coupling, which results from the interaction between the copper(II) atoms.

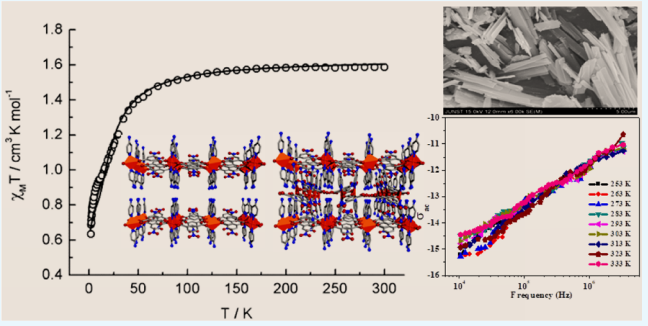

INTRODUCTION

Coordination polymers (CPs)[1−7] have been commodiously used in various fields, such as in supercapacitors,[8−11] batteries,[12] gas storage and separation, sensing,[13] and electrocatalysis.[14] But CPs with prominent magnetic and dielectric properties have garnered great attention as functional materials due to their embryonic applications in various fields, such as for electromagnetic interference shielding,[15] capacitors,[16,17] microwave tunable devices,[18,19] and broadband electric-field tunable devices.[20] Dielectric spectroscopy is routinely used to accumulate the information on the ac conduction mechanism and dielectric relaxation in an immense frequency range for different temperatures. The flexible qualitative delineation often provides new intuition into the field of dielectric behavior. For example, localized (i.e., long-range conductivity) and non-localized (i.e., dielectric relaxation) conduction processes inside the material can be esteemed by the nonexistence or existence of a relaxation peak in a frequency-dependent hypothetical modulus plot. The performance of dielectric parameter has been explored on transition metal oxide amorphous semiconductor, oxide perovskite material, ionically conducting polymer, and conducting glass.[21−23] Recently, a comprehensive study on ac conductivity and dielectric relaxation of $CH_3NH_3PbX_3$ (X = Br, I) has been reported, which shows the dominance of non-Debye-type relaxation inside the material.[24,25] In order to acquire long-range charge conduct and obvious magnetic behavior, it is pivotal for these compounds to have a tough intramolecular coupling and strong intermolecular ordering. One of the incredible characteristics of CP is its potential to acquire a distinct structural architecture under varying environments. The functional groups of the ligands and the length of the organic spacer, the reaction condition, and the nature and oxidation of metal ions immensely control the structure of the CPs. Among the 3d transition metal ions, nontoxic Cu(II) (d^9) can display a wide distinction of structures and nuclearity. The magnetic superexchange interactions in the middle of copper centers across the bridging ligands of Cu(II) compounds are established.[26,51] But the charge transfer mechanism and dielectric behavior of CPs have not been much explored. Recently, Zuo et al.[28] and Loh et al.[27] have reported the magnetic and conductivity property of copper-based CPs.

In this work, the 5-nitroisophthalate ion forms a 1D CP with Cu(II) metal node, and two axial positions are occupied by 4-aminopyridine (4-APY). The structure shows encapsulation of dinuclear Cu(II) in the 1D CP. The multinuclear Cu(II)-CP shows antiferromagnetic coupling and temperature-dependent dielectric properties.

Received: August 17, 2019
Accepted: November 13, 2019
Published: December 23, 2019

DOI: 10.1021/acsomega.9b02650
ACS Omega 2020, 5, 274−280

RESULTS AND DISCUSSION

Structure and Morphology of Compound 1, $[Cu_2(5\text{-N-IPA})_2(4\text{-APY})_4]_n$. $[Cu_2(5\text{-N-IPA})_2(4\text{-APY})_4]_n$ crystallizes in the monoclinic $P2_1/c$ space group with $Z = 4$, and the details of refinement parameters and crystal data for compound **1** are tabulated in Table S1. The structural analysis of **1** has revealed that there are two types of copper centers (Figure 1a). One of them forms a 1D polymeric network via carboxylato bridging in the square of 5-N-IPA. 4-APY is appended to the axial coordination site of Cu(II) in the dimensional network and is hydrogen bonded (3.32 Å) with the amino group of another 1D network to form a porous 2D network (Figure 1c). In the pore of this 2D network, dinuclear Cu(II) are encapsulated by the help of hydrogen bonding and $\pi\cdots\pi$ interactions (Figure 1d). The geometry around Cu centers in dinuclear Cu(II) is a distorted square pyramidal, where Cu···Cu separation lies in the range 3.388 Å.

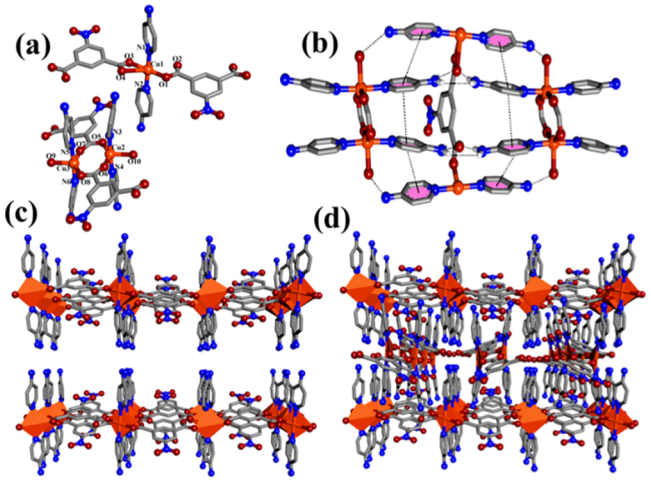

Figure 1. (a) Coordination spheres of the Cu(II) atoms, (b) schematic presentation displaying the presence of $\pi\cdots\pi$ interactions and hydrogen bonding in the compound. (c) Portion of the 2D connectivity, (d) one-dimensional Cu(II) CP with encapsulated dinuclear Cu(II).

These complexes have the potential to form higher dimensional structures throughout H-bonding (2.865−3.320 Å) and supramoleculer (aromatic $\pi\cdots\pi$) interactions (3.869−4.148 Å), (Figures 1b and S).[29−32,51,52] Some selected bond lengths and bond angles in **1** are shown in the Supporting Information (Table S2). Furthermore, the morphology of **1** was examined by field emission scanning electron microscopy (FESEM). Figure 2 displays that the nanosheets are firmly stacked and intertwined with each other.

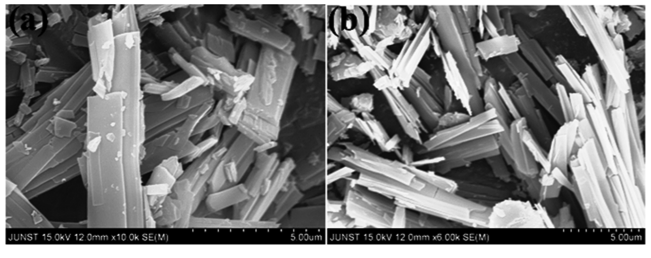

Figure 2. FESEM images of compound **1**.

Thermogravimetric Analysis and Powder X-ray Diffraction Analysis. Thermogravimetric analysis (TGA) of compound **1** is displayed showing that the compound is thermally stable up to 373 K (Figure S2). Therefore, no decomposition or deformation of compound **1** occurs at examined temperatures. The powder X-ray diffraction (PXRD) patterns of the as-synthesized compound exhibit broad diffraction peaks at 2θ (degree) as follows: 9.34, 10.55, 11.56, 14.38, 16.80, 19.48, 20.43, 22.55, 23.66, 26.28, and 30.23, which correspond to the (111), (120), (200), (102), (122), (132), (302), (042), (113), (322), and (502) planes, respectively. These were matched with the corresponding peaks of the simulated pattern, which confirmed that the bulk sample was uncontaminated (Figure S3).

Magnetic Study. The variable temperature magnetic susceptibility data for compound **1** were recorded between 300 and 2 K. A plot of $\chi_M T$ versus T is shown in Figure 3. At room temperature, $\chi_M T$ is equal to 1.586 $cm^3\ kmol^{-1}$, which is close to four uncoupled copper(II) ions with local spin $S = 1/2$ and $g \approx 2.06$.

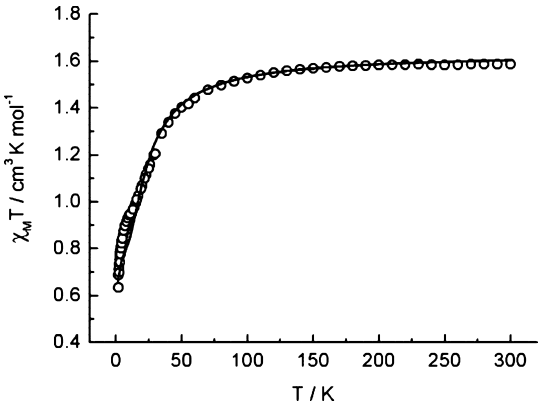

Figure 3. Plot of $\chi_M T$ vs T for compound **1** (per four Cu atoms). The solid line shows the best fit of the data (see text).

When the sample is cooled, $\chi_M T$ decreases slowly, and below 75 K, it decreases more rapidly to a value of 0.634 $cm^3\ kmol^{-1}$ at 2 K, which is slightly less for two isolated Cu(II) ions (0.75 $cm^3\ kmol^{-1}$). The shape of this curve indicates dominant antiferromagnetic coupling, which results from the interaction between the copper(II) atoms. To fit the magnetic data, we consider two of the four copper present in the elemental cell as isolated from the magnetic point of view.

The interaction through the 5-nitroisophthalate ligand in the monodimensionl fragment must be negligible (Cu···Cu = 10.225 Å) (Figure 4), thus following the Curie law for each

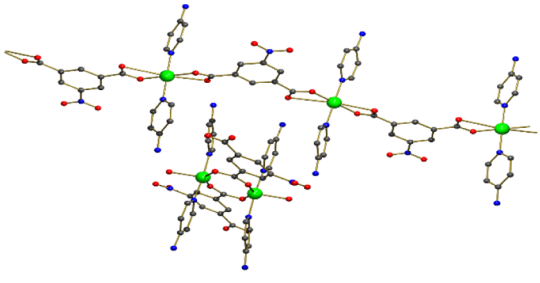

Figure 4. Structure of compound **1** showing the dinuclear and catena Cu(II) fragments formed.

DOI: 10.1021/acsomega.9b02650
ACS Omega 2020, 5, 274−280

isolated Cu(II). This part can be subtracted from the global magnetic susceptibility to give only that corresponding to the dinuclear fragment $[Cu(II)]_2$, which is aniferromagnetically coupled. Considering the above, the experimental data were fitted to the Bleaney−Bowers expression for an isotropically coupled pair of $S = 1/2$ ions (eq 1),[33] in conjunction with an additional mean field correction term, χ_{MF} (eq 2), where N is Avogadro's number, μ_B is the Bohr magneton, k is the Boltzmann constant, and z is the number of nearest neighbors.

The best least-squares fit parameters gave $J = -29.5$ cm^{-1}, $zJ' = -0.5$ cm^{-1}, $g = 2.09$, and $R = 8.21 \times 10^{-5} = \sum_i(\chi_M T_{cal} - \chi_M T_{obs})^2/(\chi_M T_{obs})^2$.

$$\chi_M = \frac{Ng^2\mu_B^2}{KT}\frac{2\exp(J/kT)}{1 + 3\exp(J/kT)} \quad (1)$$

$$\chi_{MF} = \frac{\chi_M}{1 - \chi_M\left(\frac{zJ'}{Ng^2\mu_B^2}\right)} \quad (2)$$

The field dependence of magnetization (0−5 T) measured at 2 K for compound **1** is shown in Figure 5, in the form of $M/N\mu_B$ (per Cu_4 unit) versus H/G. The magnetization reaches a value of 1.79 $M/N\mu_B$ at 5 T, which is slightly less than the expected $S = 1/2$ value of two isolated copper(II) atoms.

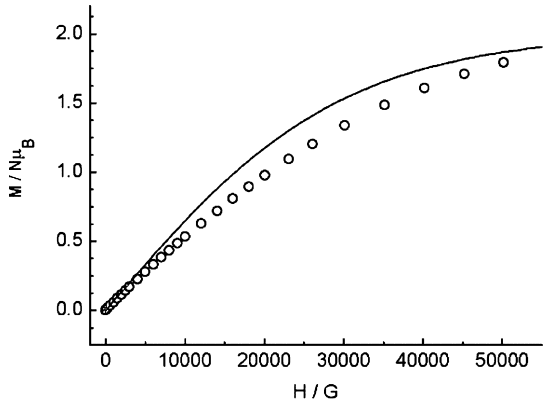

Figure 5. Field dependence of reduced magnetization at 2 K for compound **1** (per four Cu atoms); the solid line corresponds to the Brillouin function for two isolated $S = 1/2$ and $g = 2.0$.

Dielectric Studies. The complex dielectric permittivity, ε^*, of a material can be expressed as eq 3[34,35]

$$\varepsilon^*(\omega) = \varepsilon'(\omega) - j\varepsilon''(\omega) \quad (3)$$

where $\varepsilon'(\omega)$ and $\varepsilon''(\omega)$ are the real and imaginary parts of the complex dielectric constant and $\omega = 2\pi f$. Here, $\varepsilon'(\omega)$ and $\varepsilon''(\omega)$ represent the amount of electrical potential energy stored and the amount of energy dissipated due to polarization, respectively.[36,37] The real and imaginary dielectric constants of the complex can be calculated from the measured capacitance in parallel mode using eqs 4 and 5

$$\varepsilon'(\omega) = \frac{C_p d}{\varepsilon_0 A} \quad (4)$$

$$\varepsilon'(\omega) = \varepsilon''(\omega)\tan\delta \quad (5)$$

where C_p is known as the capacitance of the sample, ε_0 (8.85×10^{-14} F/cm) is the dielectric permittivity in vacuum, A is the effective surface area of the pellet, d is the thickness of the pellet, and $\tan\delta$ is the loss tangent or dissipation factor. The frequency dependence $\varepsilon'(\omega)$ for compound **1** depicts (Figure 6) that $\varepsilon'(\omega)$ decreases gradually with increasing frequency.

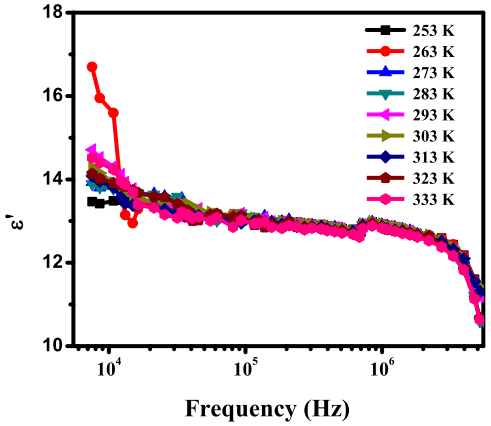

Figure 6. Frequency dependence $\varepsilon'(\omega)$ at different temperatures of compound **1**.

This behavior is in agreement with the natural properties of organic and inorganic hybrid materials.[44−47] It has been observed that at a low frequency, $\varepsilon'(\omega)$ is increased with increasing temperature. Generally, there are four types of polarization, electronic, ionic, orientation, and space charge polarization, which are mainly responsible for the high dielectric constant of the material.[35,50] This dielectric constant also strongly depends on the purity and perfection of the synthesized samples. The increase in $\varepsilon'(\omega)$ of this material may be due to the presence of metal ions with organic moieties and the non-bridging oxygen atom, which generate a dangling bond.[48,49] These metal ions contribute to the space charge polarization, which leads to the increase in $\varepsilon'(\omega)$. A small change in $\varepsilon'(\omega)$ with increasing applied temperatures is also observed for all samples, which may be due to the increase in ionic polarization in the low-frequency region.[38,39]

The frequency and temperature dependence $\varepsilon''(\omega)$ (Figure 7) for this material shows that $\varepsilon''(\omega)$ decreases with increasing frequency at all temperatures. It has been observed that $\varepsilon''(\omega)$ increases faster with temperature in the low-frequency region. TThis may be due to the potential barriers generated by the crystal defects in the material for charge transport process. As a result, the contribution of space charges becomes limited until

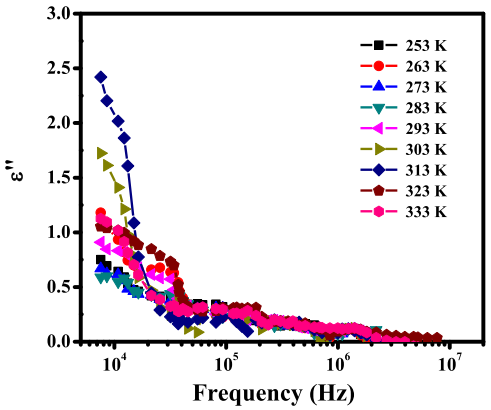

Figure 7. Frequency dependence $\varepsilon''(\omega)$ at different temperatures of compound **1**.

DOI: 10.1021/acsomega.9b02650
ACS Omega 2020, 5, 274−280

they are stopped at the grain boundary. In the low-frequency region, four types of polarizations contribute significantly to $\varepsilon''(\omega)$, but the contribution of ionic and orientational polarizations reduces in the higher frequency region. This effect decreases $\varepsilon''(\omega)$ with the increase in frequency for the examined temperatures.[40,41]

Complex Impedance Study. The complex impedance properties of compound **1** have been performed over an extensive range of frequency from 10 kHz to 5 MHz for different temperatures (253−333 K) using complex impedance spectroscopy. This is the most important method to explain the ionic movement mechanism of a material and the contribution of grain boundary and grain.[42] Detailed information about the resistive and capacitive properties of the material can be obtained from this study. The frequency-dependence complex impedance (Z^*) can be obtained using this model and is represented as eq 6

$$Z^*(\omega) = Z'(\omega) + jZ''(\omega) \quad (6)$$

where the frequency-dependence real part of impedance $Z'(\omega)$ and the imaginary part of impedance $Z''(\omega)$ can be expressed as eqs 7 and 8

$$Z'(\omega) = \frac{R_g}{[1 + (\omega R_g C_g)^2]} + \frac{R_{gb}}{[1 + (\omega R_{gb} C_{gb})^2]} \quad (7)$$

$$Z''(\omega) = \frac{\omega C_g R_g^{\,2}}{[1 + (\omega R_g C_g)^2]} + \frac{\omega C_{gb} R_{gb}^{\,2}}{[1 + (\omega R_{gb} C_{gb})^2]} \quad (8)$$

where $\omega = 2\pi f$, R_g = grain resistance, C_g = grain capacitance, R_{gb} = grain boundary resistance, and C_{gb} = grain boundary capacitance.[34,35,42]

The variation in $Z'(\omega)$ as a function of frequency and temperature (Figure 8) for compound **1** follows a sigmoidal-type pattern with an increase in the frequency. The $Z'(\omega)$ values are higher in the low-frequency region and consequently decrease with an increase in frequency and temperature. This nature reveals the increase in ac conductivity as well as the presence of the negative temperature coefficient of resistance of this material, which can generally suggest the semiconducting nature of this compound. Higher values of $Z'(\omega)$ at low frequency and temperature significantly reveal the effect of large polarization. The decrease in $Z'(\omega)$ value at a higher frequency and temperature clearly indicates the less contribution of grain boundaries in the total resistance, leading to an increase in ac conductivity with an increase in the temperature as well as frequency (Figure 9).[35]

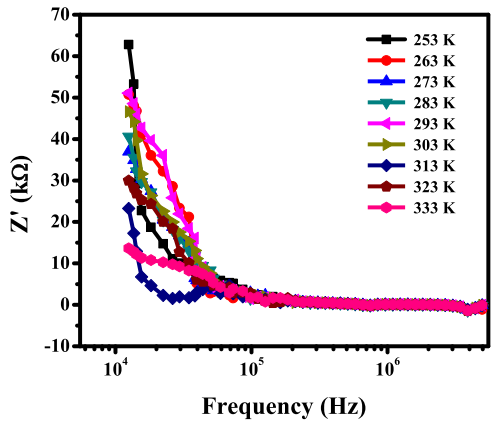

Figure 8. Frequency dependence $Z'(\omega)$ at different temperatures of compound **1**.

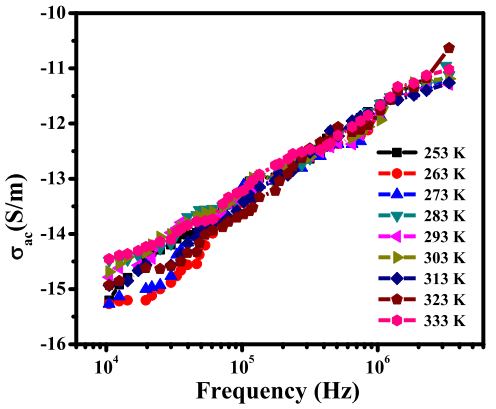

Figure 9. Frequency dependence $Z'(\omega)$ at different temperatures of compound **1**.

ac Conductivity. To explain the effect of Cu centers on the electrical conductivity of the one-dimensional Cu(II) CP with encapsulated antiferromagnetically coupled dinuclear Cu(II), the electrical conductivity measurement has also been done. Figure 10 reveals the variation in ac conductivity for compound **1**. The lower conductivity for the material could be attributed to the low level of protonation of the carboxylate, nitro, and/or amino groups of the CP. The enhancement of ac conductivity for this material comes from the effective dispersion of the compound in the matrix, which favors improved electronic transport. It can be observed that the conductivity of the one-dimensional Cu(II) CP with encapsulated antiferromagnetically coupled dinuclear Cu(II) increases with frequency and the slope becomes higher in the higher frequency region. The ac conductivity is also considered to be the combined effect of intrinsic electric dipole polarization and interface charge polarization.

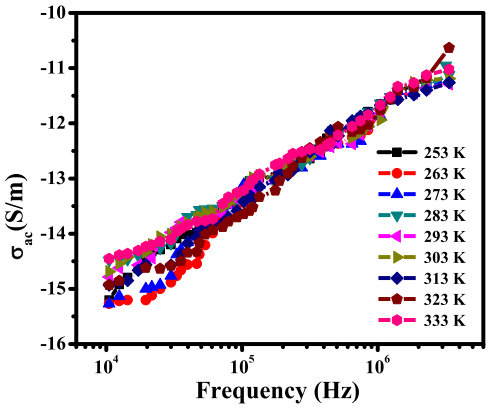

Figure 10. Frequency dependence of $\sigma_{ac}(\omega)$ at different temperatures of compound **1**.

The phenomenon appears in the metal organic polymeric system. The reason behind this is the piling of mobile charges at the interfaces, as a result of which large dipoles on metal particles or clusters are made. Polarization as well as ac conduction inside the CP is found to be dependent on the concentration of these metal particles.[34,36,43]

DOI: 10.1021/acsomega.9b02650
ACS Omega 2020, 5, 274−280

CONCLUSIONS

We have successfully synthesized one-dimensional Cu(II) CP with encapsulated antiferromagnetically coupled dinuclear Cu(II) with fascinating dielectrical and magnetic properties. The charge transfer mechanism and dielectric relaxation throughout the CP have been established. However, the overall electromagnetic properties and the effect of temperature on the electromagnetic behavior of compound **1** reveal that our as-synthesized polymer will be suitable for energy storage applications in future; still, more enhancements are yet to be done to achieve an optimized energy storage device.

EXPERIMENTAL SECTION

Materials and General Method. Sigma-Aldrich has provided all the required chemicals. Micro-analytical data (C, H, N) were collected on a PerkinElmer 2400 CHNS/O elemental analyzer. The suitable single crystal of compound **1** was used for single-crystal diffraction. A Bruker SMART APEX II diffractometer equipped with graphite-monochromated Mo Kα radiation (λ = 0.71073 Å) was used for data collection. The crystal structure was solved by the SHELX-97 package. Field emission scanning electron microscope (FESEM, S-4800, Hitachi) was used for the morphological study, and the PXRD data were collected on a Bruker D8 ADVANCE X-ray diffractometer using Cu Kα radiation (λ = 1.548 Å) generated at 40 kV and 40 mA and in a 2θ range of 5−50. Magnetic susceptibility measurements for compound **1** were carried out on polycrystalline samples, at the Servei de Magnetoquímica of the Universitat de Barcelona, with a Quantum Design SQUID MPMS-XL susceptometer apparatus working in the range 2−300 K under two magnetic field of 500 and 10 000 G. Diamagnetic corrections were estimated from Pascal tables. Frequency- and temperature-dependent electrical conductivity and dielectric properties of compound **1** were measured in the form of pellets (0.44 mm thick and 8.0 mm diameter). The samples are compressed under 5 tons/in.^{2} pressure using a hydraulic press. The pellet is placed between two copper electrodes and inserted with a holder vertically into a cylindrical furnace. All electrical measurements were done in the frequency range 10 kHz to 5 MHz in the temperature range 253−333 K using the LCR meter model Hioki IM3536. All the measurements were done at different temperatures under dark conditions, and the temperatures were controlled by an indigenous liquid nitrogen cryostat.

Synthesis of Compound. Figure 11 shows the schematic representation of the preparation of compound **1**. A methanolic solution (2 mL) of 4-APY (18.82 mg, 0.2 mmol) was judiciously layered using a water−metahnol (1:1) mixed solvent above the aqueous solution (2 mL) of $Cu(NO_3)_2\cdot 3H_2O$, (48.32 mg, 0.2 mmol). 5-Nitroisophthalic acid (5-N-IPA, 42.226 mg, 0.2 mmol) in ethanol (2 mL) was deprotonated by Et_3N (40.476 mg, 0.2 mmol) and was layered carefully above the 4-APY to build an uninterrupted layer. It was then allowed to diffuse, and the deep-blue-colored block-shaped crystals were settled on the glass wall after a week. Under a microscope, the crystals were separated and washed with methanol and water (1:1) mixed solvent and dried. The yield of $[Cu_2(5\text{-N-IPA})_2(4\text{-APY})_4]_n$, was 84% (91.84 mg). The elemental analysis for the compound was found: C, 43.87; H, 7.9; N, 14.23%.

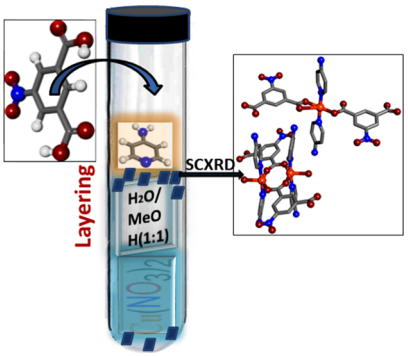

Figure 11. Schematic representation of the preparation of compound **1**.

ASSOCIATED CONTENT

Supporting Information

The Supporting Information is available free of charge at https://pubs.acs.org/doi/10.1021/acsomega.9b02650.

Supplementary structures of compound **1**, PXRD, TGA, detail of X-ray crystallographic measurements, detail of bond parameters, CCDC no. 1920033 (Figures S1−S4, Tables S1−S3) (PDF)

(CIF)

AUTHOR INFORMATION

Corresponding Authors

*E-mail: salah.elfallah@qi.ub.edu (M.S.E.F.).
*E-mail: sachindran.das@jadavpuruniversity.in (S.D.).
*E-mail: crsjuchem@gmail.com (C.S.).

ORCID

Chittaranjan Sinha: 0000-0002-4537-0609

Author Contributions

$^{\perp}$S.J. and A.R. contributed equally.

Notes

The authors declare no competing financial interest.

ACKNOWLEDGMENTS

S.J. thanks the Council of Scientific and Industrial Research (CSIR, Sanction no. 01(2894)/17/EMR-II), New Delhi, India, for financial support. M.S.E.F. acknowledges the financial support from the Spanish government (grant PGC2018-094031-B-I00).

REFERENCES

(1) Batten, S. R.; Neville, S. M.; Turner, D. R. *Coordination Polymers. Design, Analysis and Application*; Royal Society of Chemistry: London, 2009; pp 1−18.
(2) Desiraju, G. R.; Vittal, J. J.; Ramanan, A. *Crystal Engineering. A Textbook*; World Scientific: Singapore, 2011; pp 131−153.
(3) Zhou, H.-C.; Long, J. R.; Yaghi, O. M. Introduction to Metal−Organic Frameworks. *Chem. Rev.* **2012**, *112*, 673−674.
(4) Moulton, B.; Zaworotko, M. J. From molecules to crystal engineering: supramolecular isomerism and polymorphism in network solids. *Chem. Rev.* **2001**, *101*, 1629−1658.
(5) Natarajan, S.; Mahata, P.; Sarma, D. The relevance of metal organic frameworks (MOFs) in inorganic materials chemistry. *J. Chem. Sci.* **2012**, *124*, 339−353.
(6) Biradha, K.; Su, C.-Y.; Vittal, J. J. Recent developments in crystal engineering. *Cryst. Growth Des.* **2011**, *11*, 875−886.
(7) Kitagawa, S.; Kitaura, R.; Noro, S.-I. Functional porous coordination polymers. *Angew. Chem., Int. Ed.* **2004**, *43*, 2334−2375.

DOI: 10.1021/acsomega.9b02650
ACS Omega 2020, 5, 274−280

(8) Choi, K. M.; Jeong, H. M.; Park, J. H.; Zhang, Y.-B.; Kang, J. K.; Yaghi, O. M. Supercapacitors of nanocrystalline metal−organic frameworks. *ACS Nano* **2014**, *8*, 7451−7457.
(9) Yang, T.; Teng, B.; Han, S.; Li, M.; Xu, Z.; Li, Y.; Liu, Y.; Luo, J.; Sun, Z. Structural phase transition and dielectric anisotropy properties of a lead-free organic−inorganic hybrid. *Inorg. Chem. Front.* **2019**, *6*, 1761−1766.
(10) Zhao, S.; Wu, H.; Li, Y.; Li, Q.; Zhou, J.; Yu, X.; Chen, H.; Tao, K.; Han, L. Core−shell assembly of carbon nanofibers and a 2D conductive metal−organic framework as a flexible free-standing membrane for high-performance supercapacitors. *Inorg. Chem. Front.* **2019**, *6*, 1824−1830.
(11) Liu, J.; Ren, X.; Kang, X.; He, X.; Wei, P.; Wen, Y.; Li, X. Fabrication of nitrogen-rich three-dimensional porous carbon composites with nanosheets and hollow spheres for efficient supercapacitors. *Inorg. Chem. Front.* **2019**, *6*, 2082−2089.
(12) Férey, G.; Millange, F.; Morcrette, M.; Serre, C.; Doublet, M.-L.; Grenèche, J.-M.; Tarascon, J.-M. Mixed-Valence Li/Fe-Based Metal−Organic Frameworks with Both Reversible Redox and Sorption Properties. *Angew. Chem., Int. Ed.* **2007**, *46*, 3259−3263.
(13) Campbell, M. G.; Sheberla, D.; Liu, S. F.; Swager, T. M.; Dincă, M. Cu_3(hexaiminotriphenylene)$_2$: An Electrically Conductive 2D Metal−Organic Framework for Chemiresistive Sensing. *Angew. Chem., Int. Ed.* **2015**, *54*, 4349−4352.
(14) Nohra, B.; El Moll, H.; Rodriguez Albelo, L. M.; Mialane, P.; Marrot, J.; Mellot-Draznieks, C.; O'Keeffe, M.; Ngo Biboum, R.; Lemaire, J.; Keita, B.; Nadjo, L.; Dolbecq, A. Polyoxometalate-based metal organic frameworks (POMOFs): structural trends, energetics, and high electrocatalytic efficiency for hydrogen evolution reaction. *J. Am. Chem. Soc.* **2011**, *133*, 13363−13374.
(15) Bayat, M.; Yang, H.; Ko, F. K.; Michelson, D.; Mei, A. Electromagnetic interference shielding effectiveness of hybrid multi-functional Fe3O4/carbon nanofiber composite. *Polymer* **2014**, *55*, 936−943.
(16) Wuang, S. C.; Neoh, K. G.; Kang, E.-T.; Pack, D. W.; Leckband, D. E. Synthesis and functionalization of polypyrrole-Fe_3O_4 nanoparticles for applications in biomedicine. *J. Mater. Chem.* **2007**, *17*, 3354−3362.
(17) Müssig, J. H. Semiconductor capacitor with praseodymium oxide as dielectric. U.S. Patent 7,113,388 B2, 2003.
(18) Zhang, D.; Cheng, J.; Yang, X.; Zhao, B.; Cao, M. Electromagnetic and microwave absorbing properties of magnetite nanoparticles decorated carbon nanotubes/polyaniline multiphase heterostructures. *J. Mater. Sci.* **2014**, *49*, 7221−7230.
(19) Cole, M. W.; Geyer, R. G. Novel tunable acceptor doped BST thin films for high quality tunable microwave devices. *Rev. Mex. Fis.* **2004**, *50*, 232.
(20) Nair, K. M.; Guo, R.; Bhalla, A. S.; Hirano, S.-I.; Suvorov, D. *Developments in Dielectric Materials and Electronic Devices Ceramic Transactions Series*; The American Ceramic Society, 2006; Vol. *167*.
(21) Das, S.; Ghosh, A. Charge carrier relaxation in different plasticized PEO/PVDF-HFP blend solid polymer electrolytes. *J. Phys. Chem. B* **2017**, *121*, 5422−5432.
(22) Tealdi, C.; Chiodelli, G.; Malavasi, L.; Flor, G.; Fisica, C.; Unita, I. C. N. R.; Taramelli, V.; Pavia, I. Effect of alkaline-doping on the properties of La $_2$ Mo $_2$ O $_9$ fast oxygen ion conductor. *J. Mater. Chem.* **2004**, *14*, 3553−3557.
(23) Paul, T.; Ghosh, A. Structural and electrical transport properties of $La_2Mo_2O_9$ thin films prepared by pulsed laser deposition. *J. Appl. Phys.* **2017**, *121*, 135106.
(24) Sheikh, M. S.; Sakhya, A. P.; Dutta, A.; Sinha, T. P. Dielectric relaxation of $CH_3NH_3PbI_3$ thin film. *Thin Solid Films* **2017**, *638*, 277−281.
(25) Sheikh, M. S.; Sakhya, A. P.; Sadhukhan, P.; Dutta, A.; Das, S.; Sinha, T. P. Dielectric relaxation and Ac conductivity of perovskites $CH_3NH_3PbX_3$ (X = Br, I). *Ferroelectrics* **2017**, *514*, 146−157.
(26) Mohideen, M. I. H.; Lei, C.; Tucek, J.; Malina, O.; Brivio, F.; Kasneryk, V.; Huang, Z.; Mazur, M.; Zou, X.; Nachtigall, P.; Cejkaa, J.; Morris, R. E. Magneto-structural correlations of novel kagomé-type metal organic frameworks. *J. Mater. Chem. C* **2019**, *7*, 6692−6697.
(27) Sengupta, A.; Datta, S.; Su, C.; Herng, T. S.; Ding, J.; Vittal, J. J.; Loh, K. P. Tunable Electrical Conductivity and Magnetic Property of the Two Dimensional Metal Organic Framework [Cu(TPyP)-$Cu_2(O_2CCH_3)_4$]. *ACS Appl. Mater. Interfaces* **2016**, *8*, 16154−16159.
(28) Yu, F.; Kurmoo, M.; Zhuang, G.-L.; Zuo, J.-L. Hierarchical tandem assembly of planar [3× 3] building units into {3×[3× 3]} oligomers: mixed-valency, electrical conductivity and magnetism. *Chem. Sci.* **2018**, *9*, 7498−7504.
(29) Naskar, K.; Dey, A.; Dutta, B.; Ahmed, F.; Sen, C.; Mir, M. H.; Roy, P. P.; Sinha, C. Intercatenated coordination polymers (ICPs) of carboxylato bridged Zn (II)-isoniazid and their electrical conductivity. *Cryst. Growth Des.* **2017**, *17*, 3267−3276.
(30) Naskar, K.; Maity, S.; Jana, S.; Dutta, B.; Tanaka, S.; Mallick, D.; Akitsu, T.; Sinha, C. Arylazoimidazole Coordinated and Naphthalene-Dicarboxylato Bridged Polymers of Co (II) and Photochromic Zn (II) Complexes. *Cryst. Growth Des.* **2018**, *18*, 2986−2997.
(31) Siddiqui, M. M.; Saha, R.; Mukherjee, P. S. Ruthenium(II) Metalla[2]catenanes and Macrocycles via Donor-Dependent Self-Assembly. *Inorg. Chem.* **2019**, *58*, 4491−4499.
(32) Dutta, B.; Jana, R.; Bhanja, A. K.; Ray, P. P.; Sinha, C.; Mir, M. H. Supramolecular aggregate of Cadmium (II)-based one-dimensional coordination polymer for device fabrication and sensor application. *Inorg. Chem.* **2019**, *58*, 2686−2694.
(33) Bleaney, B.; Bowers, K. D. Anomalous paramagnetism of copper acetate. *Proc. R. Soc. London, Ser. A* **1952**, *214*, 451−465.
(34) Maji, P.; Ray, A.; Sadhukhan, P.; Chatterjee, S.; Das, S. Study on charge transfer mechanism and dielectric relaxation of cesium lead bromide (CsPbBr3). *J. Appl. Phys.* **2018**, *124*, 124102.
(35) Ray, A.; Roy, A.; Bhattacharjee, S.; Jana, S.; Ghosh, C. K.; Sinha, C.; Das, S. Correlation between the dielectric and electro-chemical properties of TiO2-V2O5 nanocomposite for energy storage application. *Electrochim. Acta* **2018**, *266*, 404−413.
(36) Maji, P.; Chatterjee, S.; Das, S. Study on charge transportation and scaling behavior of $CsPbI_3$ microwires. *Ceram. Int.* **2019**, *45*, 6012−6020.
(37) Dhara, A.; Sain, S.; Das, S.; Pradhan, S. K. Microstructure, optical and electrical characterizations of Mn doped ZnS nanocrystals synthesized by mechanical alloying. *Mater. Res. Bull.* **2018**, *97*, 169−175.
(38) Acharya, T.; Choudhary, R. N. P. Dielectric and electrical characteristics of $La_{0.5}Na_{0.5}Ga_{0.5}V_{0.5}O_3$. *Phys. Lett. A* **2016**, *380*, 2437−2444.
(39) Mandal, S. K.; Singh, S.; Dey, P.; Roy, J. N.; Mandal, P. R.; Nath, T. K. Frequency and temperature dependence of dielectric and electrical properties of TFe_2O_4 (T= Ni, Zn, $Zn_{0.5}Ni_{0.5}$) ferrite nanocrystals. *J. Alloys Compd.* **2016**, *656*, 887−896.
(40) Das, M. R.; Mukherjee, A.; Mitra, P. Structural, optical and ac electrical characterization of CBD synthesized NiO thin films: Influence of thickness. *Phys. E* **2017**, *93*, 243−251.
(41) Jana, P. K.; Mukherjee, S.; Chaudhuri, B. K. Existence of internal domains in LixTiyNi1− x− yO and their effects on dielectric behaviour. *J. Phys. D: Appl. Phys.* **2014**, *47*, 365302.
(42) Fang, T.-T.; Liu, C. P. Evidence of the Internal Domains for Inducing the Anomalously High Dielectric Constant of $CaCu_3Ti_4O_{12}$. *Chem. Mater.* **2005**, *17*, 5167−5171.
(43) Dong, W.; Hu, W.; Berlie, A.; Lau, K.; Chen, H.; Withers, R. L.; Liu, Y. Colossal Dielectric Behavior of Ga+Nb Co-Doped Rutile TiO_2. *ACS Appl. Mater. Interfaces* **2015**, *7*, 25321−25325.
(44) Galli, S.; Cimino, A.; Ivy, J. F.; Giacobbe, C.; Arvapally, R. K.; Vismara, R.; Checchia, S.; Rawshdeh, M. A.; Cardenas, C. T.; Yaseen, W. K.; Maspero, A.; Omary, M. A. Fluorous Metal−Organic Frameworks and Nonporous Coordination Polymers as Low-κ Dielectrics. *Adv. Funct. Mater.* **2019**, *29*, 1904707.
(45) Balendra; Banday, A.; Tewari, S.; Singh, B.; Murugavel, S.; Ramanan, A. Alkaline-earth metal based coordination polymers

DOI: 10.1021/acsomega.9b02650
ACS Omega 2020, 5, 274−280

assembled from two different V-shaped ligands: Synthesis, structure, and dielectric properties. *Inorg. Chim. Acta* **2019**, *495*, 118940.
(46) Ashalatha, A.; Sudarsanakumar, M. R.; Shibu Prasad, S.; Suma, S.; Prathapachandra Kurup, M. R.; Rahul, S. Synthesis, crystal structure and dielectric properties of a new acetate bridged coordination polymer: $\{[La(\mu\text{-}CH_3COO)(PDC)(H_2O)_2].2H_2O\}_n$. *J. Mol. Struct.* **2019**, *1195*, 522−527.
(47) Zhang, M.; Tan, Y.-L.; Chen, X.-R.; Yu, H.; Zhang, W.-H.; Lang, J.-P. A cationic [Ag12S12] cluster-based 2D coordination polymer and its dye composite with enhanced photocurrent and dielectric responses. *Dalton Trans.* **2019**, *48*, 8546−8550.
(48) Balendra; Banday, A.; Kumar, V.; Murugavel, S.; Ramanan, A. Strontium-Carboxylate-Based Coordination Polymers: Synthesis, Structure and Dielectric Properties. *ChemistrySelect* **2019**, *4*, 4756−4766.
(49) Sima, J.-Y.; Li, H.-X.; Young, D. J.; Braunstein, P.; Lang, J.-P. Reversible dielectric switching behavior of a 1D coordination polymer induced by photo and thermal irradiation. *Chem. Commun.* **2019**, *55*, 3532−3535.
(50) Kao, Y.-C.; Mendiratta, S.; Usman, M.; Wen, Y. S.; Wang, C. M.; Zhao, L.; Wu, M. K.; Lu, K. L. Exceptional Low Dielectric Behavior of Chemically Robust, Guest-Free Co- and Mn-Based Coordination Polymers. *ChemElectroChem* **2019**, *6*, 623−626.
(51) Jana, S.; Jana, R.; Sil, S.; Dutta, B.; Sato, H.; Ray, P. P.; Datta, A.; Akitsu, T.; Sinha, C. Influence of Axial Linkers on Polymerization in Paddle-Wheel Cu(II) Coordination Polymers for the Application of Optoelectronics Devices. *Cryst. Growth Des.* **2019**, *19*, 6283−6290.
(52) Chandra, A.; Das, M.; Pal, K.; Jana, S.; Dutta, B.; Ray, P. P.; Jana, K.; Sinha, C. Three-Dimensional-Coordination Polymer of Zn(II)-Carboxylate: Structural Elucidation, Photoelectrical Conductivity, and Biological Activity. *ACS Omega* **2019**, *4*, 17649−17661.

DOI: 10.1021/acsomega.9b02650
ACS Omega 2020, 5, 274−280